Effective medium theory for graphene-covered metallic gratings

2016 J. Opt. 18 105005

(http://iopscience.iop.org/2040-8986/18/10/105005)

IOP Publishing Journal of Optics
J. Opt. 18 (2016) 105005 (8pp) doi:10.1088/2040-8978/18/10/105005

Effective medium theory for graphene-covered metallic gratings

Babak Rahmani, Amirmasood Bagheri, Amin Khavasi and Khashayar Mehrany

Department of Electrical Engineering, Sharif University of Technology, Tehran, Iran

E-mail: khavasi@sharif.edu

Received 12 May 2016, revised 30 July 2016
Accepted for publication 17 August 2016
Published 20 September 2016

Abstract

We propose an effective medium theory for a one-dimensional periodic array of rectangular grooves covered by a graphene sheet. Parameters of the effective medium model are given by explicit analytical expressions for both major polarizations TM and TE, and for all incident angles. In extraction of this model, we assumed single mode approximation inside the grooves. The effect of non-specular diffraction orders outside the grating, as well as the plasmonic response of the graphene sheet in the far-infrared spectrum, is addressed by introducing an effective surface conductivity at the interface of the metallic grating and the ambient environment. It is shown that surface plasmons in graphene effectively capture diffracted waves in the metallic grating leading to near total absorption. Results of this work may pave the way for designing wide-band absorbers for terahertz applications.

Keywords: graphene, metallic grating, effective medium theory

(Some figures may appear in colour only in the online journal)

1. Introduction

Graphene, a one-atom thick carbon layer material arranged in a honeycomb lattice, has attracted huge research interest due to its exceptional electrical and optical properties including optical transparency [1], high electrical conductivity [2] and controllable plasmonic properties [3]. Graphene is used in a variety of applications such as transformation optics [4], transparent electrodes [5] and high-speed photo-detectors [6].

Enhancing the absorption of graphene has recently attracted a noticeable amount of attention [7–18]. The plasmonic response of graphene plays a crucial role in the absorption process, because the incident wave is coupled to the plasmonic modes of graphene leading to strong absorption. However, it should be noticed that at higher frequencies (with respect to the Fermi level of graphene) the plasmonic response disappears because of dominancy of the interband transition term. This usually happens at the near-infrared and visible range [7]. On the other hand, intraband transition is a key factor in the far-infrared (FIR) wavelength region [7]. Consequently, the absorption of graphene can be significantly enhanced in the FIR by exploiting the plasmonic response of graphene, which is controllable through electrical gating or chemical doping [2].

Due to low absorption of a single layer graphene, other mechanisms are required to enhance the absorption. In patterned graphene structures such as disks, ribbons and patch arrays, incident light is captured by localized plasmons and consequently, even a total absorption is achievable [19–23]. Moreover, absorption enhancement can be obtained through the synergistic combination of graphene with other structures such as photonic crystals [8] and metallic gratings [9, 10]. Using the above-mentioned mechanisms, i.e. the combination of graphene with metallic structures which are used as substrates, may lead to the realization of an efficient absorber for FIR and low terahertz (THz) frequency regions [9, 10]. The aim of this work is to propose an analytical effective medium theory for a metallic grating covered by a graphene sheet.

Since the discovery of extraordinary transmission (EOT) [24], structured metallic systems have been under intensive study. Several analytical and numerical techniques have been provided in the literature for the analysis of metallic gratings [25–31].

In this paper, absorption enhancement of a structure composed of a graphene sheet on top of a periodic arrangement of rectangular grooves perforated in a metallic slab is investigated. The metallic regions can be approximated by a perfect electric conductor (PEC) in the THz frequency regime. It will be shown that the incident power can be completely absorbed by tailoring the plasmonic response of graphene in the THz frequency region. To this end, we propose an effective medium model that mimics the graphene-covered metallic gratings for both major polarizations transverse magnetic (TM) and transverse electric (TE) and for any arbitrary incident angle. This effective medium model consists of a slab with an effective permittivity that is placed on top of a bulk metallic layer. The effect of the graphene sheet as well as the effect of non-specular diffracted waves in the metallic grating can be accounted for by introducing an effective surface conductivity at the interface of the effective medium model and the ambient environment. It should be pointed out that a similar effective medium theory has been proposed for one-dimensional slits carved in metallic film but without graphene [26]. Furthermore, that model has been only derived for the TM illumination and is limited to the cases in which the ambient environment and the groove regions are vacuum. The accuracy of the proposed effective medium theory is verified by comparing the reflected power obtained by the proposed model with that of the full-wave numerical simulations using the commercial software COMSOL Multiphysics. By virtue of this model, we are able to investigate the effect of geometry on absorption and this facilitates designing absorbers with near perfect absorption in the THz frequency regime. Additionally, the here-proposed effective medium model can be used to study how EOT can be tailored by using graphene.

The paper is organized as follows: section 2 is devoted to the detailed description of the proposed effective medium model. In section 3, numerical examples are given to show the validity of the model. Also, characteristics of an efficient absorber and the effect of geometrical parameters on the absorption enhancement are discussed using the proposed model. Finally, conclusions are drawn in section 4. A time dependence of the form $e^{j\omega t}$ is assumed throughout this paper.

2. Effective medium model

In this section, we propose the effective medium theory for one-dimensional metallic gratings covered by a graphene sheet. The schematic of the structure is shown in figure 1. The one dimensional grating is periodic with period d in x-direction. Note that the structure is extended to infinity in the y-direction. The width and height of the grooves are a and h, respectively. For analytical calculations, the graphene sheet is modeled as a conductive layer with conductivity σ_g, which modifies the boundary condition of the magnetic fields. The conductivity of graphene is derived using the well-known

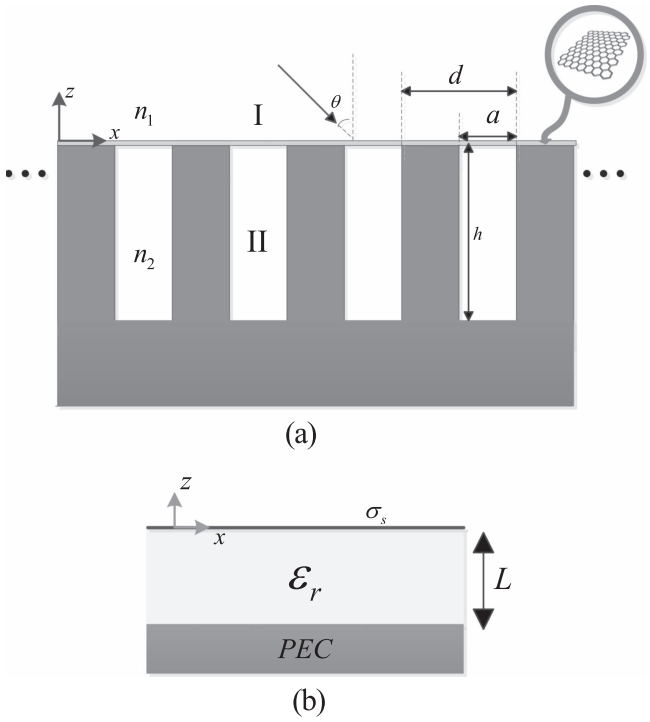

Figure 1. (a) Metallic grating covered by a graphene sheet and illuminated by a plane wave. The region above the grating and the grooves region are denoted by I and II, respectively. (b) The effective medium model proposed for the structure depicted in (a).

Kubo formula [18] and can be written as follow:

$$\sigma_g = \frac{2e^2 k_B T}{\pi \hbar^2}\frac{j}{j\tau^{-1}-\omega}\ln\left[2\cosh\left(E_F/2k_BT\right)\right] - \frac{je^2}{4\pi\hbar}\ln\left[\frac{2E_F-\hbar(\omega-j\tau^{-1})}{2E_F+\hbar(\omega-j\tau^{-1})}\right] \quad (1)$$

where e is the electron charge, E_F is the Fermi energy, $\hbar$ is the reduced Planck constant, ω is the angular frequency, $T = 300\,\mathrm{K}$ is the temperature and τ is the relaxation time. For low THz frequencies (where the interband part of the conductivity in (1) can be neglected) and for $E_F \gg k_B T$, the graphene surface conductivity σ_g is well described by the Drude form [21]:

$$\sigma_g = \frac{e^2 E_F}{\pi\hbar^2}\frac{j}{j\tau^{-1}-\omega}. \quad (2)$$

In the rigorous full-wave calculations carried out by COMSOL Multiphysics, graphene is modeled by an ultrathin ($\Delta = 1\,\mathrm{nm}$) layer whose permittivity is $\varepsilon_g = \varepsilon_0 - j\sigma_g/(\omega\Delta)$ [18].

In the following subsections, we derive the equivalent model for the structure in figure 1 for both polarizations TM and TE.

2.1. TM polarization

First assume that the structure depicted in figure 1(a) is illuminated by a TM polarized wave (the magnetic field in the y-direction) with incident angle θ with respect to the

z-direction. The tangential electric and magnetic fields of the incident wave in region I can be written as

$$H_{1y} = H_{10}^{+}\mathrm{e}^{jk_{z10}z}\mathrm{e}^{-jk_{x10}x} + \sum_{n} H_{1n}^{-}\mathrm{e}^{-jk_{z1n}z}\mathrm{e}^{-jk_{x1n}x} \tag{3a}$$

$$E_{1x} = -\xi_{10}H_{10}^{+}\mathrm{e}^{jk_{z10}z}\mathrm{e}^{-jk_{x10}x} + \sum_{n}\xi_{1n}H_{1n}^{-}\mathrm{e}^{-jk_{z1n}z}\mathrm{e}^{-jk_{x1n}x}. \tag{3b}$$

In the above equations, the subscript n corresponds to the order of the diffracted wave. Also, k_{x1n} and k_{z1n} are wave-vector components in the $\hat{x}$ and $\hat{z}$ directions in region I, which are given by

$$k_{x1n} = k_{x10} + \frac{2n\pi}{d},\ k_{x10} = k_0 n_1 \sin\theta \quad n = 0,\ \pm1,\ \pm2,\ \ldots \tag{4}$$

$$k_{z1n} = k_0\sqrt{n_1^2 - (n_1\sin\theta + n\lambda/d)^2}\,,\ \mathrm{Im}[k_{z1n}] < 0, \quad n = 0,\ \pm1,\ \pm2,\ .. \tag{5}$$

where $k_0 = 2\pi/\lambda$ is the wave-number in the free space and λ is the free space wavelength. Moreover, $\xi_{1n} = k_{z1n}/\omega\varepsilon_1$ is the TM impedance of the nth diffracted order in region I. In region II, we assume that only the fundamental transverse electromagnetic (TEM) mode is propagating inside the grooves and we neglect the effects of higher order modes. This assumption requires that $\lambda > 2an_2$ [30]. Consequently, the electromagnetic fields in region II can be written in the form

$$H_{2y} = H_{20}^{+}(\mathrm{e}^{j\beta z} + \mathrm{e}^{-j\beta(z+2h)}) \tag{6a}$$

$$E_{2x} = -\xi_{20}H_{20}^{+}(\mathrm{e}^{j\beta z} - \mathrm{e}^{-j\beta(z+2h)}) \tag{6b}$$

where

$$\xi_{20} = \frac{\beta}{\omega\varepsilon_2}, \quad \beta = k_0 n_2. \tag{7}$$

Applying the boundary conditions for tangential electric fields at the interface between the two regions yields

$$H_{10}^{+} - H_{10}^{-} = H_{20}^{+}\frac{\xi_{20}}{\xi_{10}}\sqrt{\frac{a}{d}}\,p_0^{+}(1 - \mathrm{e}^{-j2\beta h}) \tag{8a}$$

$$H_{1n}^{-} = -H_{20}^{+}\frac{\xi_{20}}{\xi_{1n}}\sqrt{\frac{a}{d}}\,p_n^{+}(1 - \mathrm{e}^{-j2\beta h}), \quad n \neq 0 \tag{8b}$$

where

$$p_n^{\pm} = \frac{1}{\sqrt{ad}}\int_0^a \mathrm{e}^{\pm jk_{x1n}x}\mathrm{d}x. \tag{9}$$

These equations are obtained by multiplying the electric fields by $\mathrm{e}^{+jk_{x1n}x}$ and integrating both sides over one period. On the other hand, for the tangential magnetic fields, the boundary condition at $z = 0$ reads as

$$H_{10}^{+}p_0^{-} + \sum_{n} H_{1n}^{-}p_n^{-} = H_{20}^{+}\sqrt{\frac{a}{d}}\,[(1 + \sigma_g\xi_{20}) + \mathrm{e}^{-j2\beta h}(1 - \sigma_g\xi_{20})] \tag{10}$$

where the effect of graphene surface conductivity is included. This relation is obtained by integrating both sides over one groove width. By rearranging (8) and (10), and after some straightforward mathematical manipulations, one finds the following expression for the reflection coefficient

$$\Gamma_0^{\mathrm{TM}} = \frac{(1 + \phi_1^{-})\mathrm{e}^{+j\beta h} + (1 - \phi_1^{-})\mathrm{e}^{-j\beta h}}{(1 + \phi_1^{+})\mathrm{e}^{+j\beta h} + (1 - \phi_1^{+})\mathrm{e}^{-j\beta h}} \tag{11}$$

where $\Gamma_0^{\mathrm{TM}} = \dfrac{H_{10}^{-}}{H_{10}^{+}}$ and

$$\phi_1^{\pm} = \xi_{20}\left(\sigma_g \pm \frac{|p_0^{+}|^2}{\xi_{10}} + \sum_{n\neq 0}\frac{|p_n^{+}|^2}{\xi_{1n}}\right). \tag{12}$$

(11) is similar to the reflection coefficient of the dielectric slab model shown in figure 1(b), which is [26]

$$\Gamma^{\mathrm{TM}} = \frac{(1 + \phi_2^{-})\mathrm{e}^{+jk_z L^{\mathrm{TM}}} + (1 - \phi_2^{-})\mathrm{e}^{-jk_z L^{\mathrm{TM}}}}{(1 + \phi_2^{+})\mathrm{e}^{+jk_z L^{\mathrm{TM}}} + (1 - \phi_2^{+})\mathrm{e}^{-jk_z L^{\mathrm{TM}}}} \tag{13}$$

where

$$\phi_2^{\pm} = \frac{\sigma_s k_z}{\omega\varepsilon_0\varepsilon_r^{\mathrm{TM}}} \pm \frac{k_z}{\omega\varepsilon_0\varepsilon_r^{\mathrm{TM}}\xi_{10}} \tag{14a}$$

and

$$k_z = \sqrt{k_0^2\varepsilon_r^{\mathrm{TM}} - k_{x10}^2} \tag{14b}$$

in which, k_{x10} is given in (4). By comparing the two coefficients Γ_0^{TM} and Γ^{TM}, we are able to find an expression for the effective surface conductivity, the effective relative permittivity and the effective height of the slab:

$$\sigma_s^{\mathrm{TM}} = \frac{\sigma_g}{|p_0^{+}|^2} + \sum_{n\neq 0}\frac{|p_n^{+}|^2}{|p_0^{+}|^2}\frac{1}{\xi_{1n}} \tag{15}$$

$$\varepsilon_r^{\mathrm{TM}} = \frac{1 + \left(1 - 4\dfrac{|p_0^{+}|^4}{n_2^2}\sin^2\theta\right)^{1/2}}{2\dfrac{|p_0^{+}|^4}{n_2^2}} \tag{16}$$

and

$$L^{\mathrm{TM}} = \frac{2\dfrac{|p_0^{+}|^2}{n_2}h}{1 + \left(1 - 4\dfrac{|p_0^{+}|^4}{n_2^2}\sin^2\theta\right)^{1/2}} \tag{17}$$

respectively. (16) and (17) can be further simplified for incident angles near zero. For normally incident waves, $|p_0^{+}|^2 = a/d$ and thus we have $\varepsilon_r^{\mathrm{TM}} = (d/a)^2 n_2^2$ and $L^{\mathrm{TM}} = h/n_2 \times a/d$. It is worth mentioning that similar expressions have been reported in [26] for L^{TM}, $\varepsilon_r^{\mathrm{TM}}$ and surface conductivity σ_s^{TM} in the absence of a graphene sheet, however inserting the conductivity of graphene, i.e. σ_g, into the equations only changes the effective surface conductivity σ_s^{TM}. In other words, the graphene conductivity with a simple factor d/a at normal incidence is added to the artificial surface conductivity reported in [26]. The imaginary parts of the two terms in (15) have different signs in the subwavelength regime and thus, at their resonant frequencies, they

cancel out each other leading to a pure real conductivity. This pure real conductivity is essential for strong absorption. This phenomenon can be elucidated in different fashions [9–12]. Recently, it was demonstrated that the above mentioned resonant frequency of the enhanced absorption in the graphene-covered metallic grating can be predicted by using an inductor-capacitor (LC) model [10–12]. It was also shown that the grating produces a strong localized electric field at these resonant frequencies which is referred to as magnetic polariton (MP). The coupling of MPs with the plasmonic resonance in the graphene sheet is responsible for the enhanced absorption of the graphene-covered metallic grating [10, 11].

It is noteworthy to mention that our proposed model also allows the local fields to be identified using the Rayleigh expansion for the electromagnetic fields outside the grating. The coefficients of this expansion can be calculated from (8). Additionally, the dissipation can be also incorporated into the model using complex propagation constants for the mode inside the grooves [27].

2.2. TE polarization

In this part, we carry out a similar analysis to that of the previous part for TM polarization, but assuming that the structure is illuminated by a TE polarized wave (the electric field in the y-direction) with incident angle θ with respect to the z-direction. Therefore, the tangential electric and magnetic fields of the incident wave in region I are

$$E_{1y} = E_{10}^{+}\mathrm{e}^{jk_{z10}z}\mathrm{e}^{-jk_{x10}x} + \sum_{n} E_{1n}^{-}\mathrm{e}^{-jk_{z1n}z}\mathrm{e}^{-jk_{x1n}x} \tag{18a}$$

$$H_{1x} = \varsigma_{10}E_{10}^{+}\mathrm{e}^{jk_{z10}z}\mathrm{e}^{-jk_{x10}x} - \sum_{n}\varsigma_{1n}E_{1n}^{-}\mathrm{e}^{-jk_{z1n}z}\mathrm{e}^{-jk_{x1n}x} \tag{18b}$$

where k_{x1n} and k_{z1n} are defined by (4) and (5) and $\varsigma_{1n} = k_{z1n}/\omega\mu$ is the TE admittance of the nth diffracted order in region I. Similar to the previous section, we assume that only the fundamental TE mode propagates inside the grooves. This assumption is valid as long as all higher order modes are in cut-off. So, the condition $\lambda > an_2$ must be satisfied [30]. As a result, the electromagnetic fields in region II are given by

$$E_{2y} = E_{20}^{+}\sin\left(\frac{\pi x}{a}\right)(\mathrm{e}^{j\beta z} - \mathrm{e}^{-j\beta(z+2h)}) \tag{19a}$$

$$H_{2x} = \varsigma_{20}\,E_{20}^{+}\sin\left(\frac{\pi x}{a}\right)(\mathrm{e}^{j\beta z} + \mathrm{e}^{-j\beta(z+2h)}) \tag{19b}$$

where

$$\varsigma_{20} = \frac{\beta}{\omega\mu}, \quad \beta = \sqrt{(k_0 n_2)^2 - (\pi/a)^2}\,. \tag{20}$$

Applying the continuity of the tangential electric fields at the interface between the two regions yields:

$$E_{10}^{+} + E_{10}^{-} = E_{20}^{+}\sqrt{\frac{a}{2d}}\,q_0^{+}(1 - \mathrm{e}^{-j2\beta h}) \tag{21a}$$

$$E_{1n}^{-} = E_{20}^{+}\sqrt{\frac{a}{2d}}\,q_n^{+}(1 - \mathrm{e}^{-j2\beta h}), \quad n \neq 0 \tag{21b}$$

where

$$q_n^{\pm} = \sqrt{\frac{2}{ad}}\int_0^a \sin\left(\frac{\pi x}{a}\right)\mathrm{e}^{\pm jk_{x1n}x}\mathrm{d}x. \tag{22}$$

It should be noted that these relations are obtained by multiplying the electric fields by $\mathrm{e}^{+jk_{x1n}x}$ and integrating both sides over one period. Similarly, we have:

$$E_{10}^{+}\varsigma_{10}\,q_0^{-} - \sum_{n}E_{1n}^{-}\varsigma_{1n}q_n^{-} = E_{20}^{+}\sqrt{\frac{a}{2d}}\,[(\sigma_g + \varsigma_{20}) - \mathrm{e}^{-j2\beta h}(\sigma_g - \varsigma_{20})] \tag{23}$$

which is obtained by applying the boundary condition for the tangential magnetic fields at $z = 0$. This relation is obtained by multiplying the magnetic fields by $\sin(\pi x/a)$ and integrating both sides over one groove width. By rearranging and simplifying (21) and (23), the following expression is derived for the reflection coefficient:

$$\Gamma_0^{\mathrm{TE}} = \frac{-(\varphi_1^{-} + 1)\mathrm{e}^{+j\beta h} + (\varphi_1^{-} - 1)\mathrm{e}^{-j\beta h}}{(\varphi_1^{+} + 1)\mathrm{e}^{+j\beta h} - (\varphi_1^{+} - 1)\mathrm{e}^{-j\beta h}} \tag{24}$$

where $\Gamma_0^{\mathrm{TE}} = \dfrac{E_{10}^{-}}{E_{10}^{+}}$ and

$$\varphi_1^{\pm} = \frac{1}{\varsigma_{20}}\left(\sigma_g \pm \varsigma_{10}\,|q_0^{+}|^2 + \sum_{n\neq 0}\varsigma_{1n}\,|q_n^{+}|^2\right). \tag{25}$$

The above equation is similar to the reflection coefficient of the dielectric slab model shown in figure 1(b), which is

$$\Gamma^{\mathrm{TE}} = \frac{-(\varphi_2^{-} + 1)\mathrm{e}^{+jk_z L^{\mathrm{TE}}} + (\varphi_2^{-} - 1)\mathrm{e}^{-jk_z L^{\mathrm{TE}}}}{(\varphi_2^{+} + 1)\mathrm{e}^{+jk_z L^{\mathrm{TE}}} - (\varphi_2^{+} - 1)\mathrm{e}^{-jk_z L^{\mathrm{TE}}}} \tag{26}$$

where

$$\varphi_2^{\pm} = \frac{\sigma_s\omega\mu}{k_z} \pm \frac{k_{z10}}{k_z} \tag{27a}$$

and

$$k_z = \sqrt{k_0^2\,\varepsilon_r^{\mathrm{TE}} - k_{x10}^2} \tag{27b}$$

in which, k_{x10} is defined by (4). By comparing the two coefficients Γ_0^{TE} and Γ^{TE}, we are able to find an expression for the effective surface conductivity, the effective relative permittivity and the effective height of the slab:

$$\sigma_s^{\mathrm{TE}} = \frac{\sigma_g}{|q_0^{+}|^2} + \sum_{n\neq 0}\varsigma_{1n}\frac{|q_n^{+}|^2}{|q_0^{+}|^2} \tag{28}$$

$$\varepsilon_r^{\mathrm{TE}} = \left(\frac{\pi^2 d}{8a}\right)^2\left(n_2^2 - \frac{\omega_p^2}{\omega^2}\right) + \sin^2\theta \tag{29}$$

and

$$L^{\mathrm{TE}} = h\left(\frac{\pi^2 d}{8a}\right)^{-1} \tag{30}$$

where $\omega_p = \pi c/a$ is the plasma-like frequency and c is the speed of light in the free space. Note that the approximation $1/|q_0^{+}|^2 \approx \pi^2 d/(8a)$ is used to simplify (29) and (30). It is

worth mentioning that the imaginary parts of the two terms in the surface conductivity, given in (28), have the same signs in the subwavelength regime. Hence, pure real surface conductivity and thus strong absorption are not expected for this polarization. Accordingly, it is explained in [12] that the TE waves cannot excite MPs in the one-dimensional grating and consequently enhanced graphene absorption is absent for this polarization state.

3. Results and discussion

We present several numerical examples to verify the accuracy of the proposed model. We use COMSOL Multiphysics for the rigorous full-wave analysis. The maximum element size in the finite element method should be small enough ($\sim\lambda/18$, where λ is the wavelength of the free space) to ensure convergence. On the other hand, the series with infinite terms in (15) and (28) have to be inevitably truncated for practical reasons. However, keeping about seven terms is usually enough for the results to converge.

In this section, the analytical solution based on the single mode approximation within each groove, i.e. (11) for the TM waves and (24) for the TE waves, is calculated and compared against results of the full-wave simulations and the proposed model. As the first numerical example, we suppose that the structure is illuminated by a TM polarized wave incident at angles $\theta = 0^\circ$ and $\theta = 60^\circ$. The parameters of the structure are $n_1 = 1$, $n_2 = 1$, $d = 200\ \mu$m, $h = 100\ \mu$m and $a = 50\ \mu$m. Based on the definition of the normalized frequency (d/λ), the working frequency range of this example is 0–3.75 THz. Furthermore, the Fermi energy of graphene is set to $E_F = 0.1$ eV hereafter unless otherwise specified.

In figure 2, the reflected power obtained by the rigorous full-wave analysis (solid line), the analytical solution based on the TEM single mode approximation inside the grooves, i.e. (11), (dotted line) and the proposed effective medium model (dashed line) is plotted versus the normalized frequency. Additionally, the maximum frequency limit in which the proposed model is valid based on the single mode condition within each groove, i.e. $\lambda > 2an_2$, is marked with a straight dashed line. The proposed model is in excellent agreement with the other two methods for the normalized frequencies well below this limit. Interestingly, for normally incident waves, this model remains accurate for the normalized frequencies larger than the above-mentioned limit. Because the higher order mode in the parallel plate waveguide formed by the metallic walls in the grooves has an odd symmetry and cannot be excited at normal incidence.

As is obvious in figure 2, the model loses it accuracy at higher frequencies for oblique incidence angles. This is due to the considerable contribution of evanescent modes inside the grooves which can be strongly excited at oblique incidence. For large values of a/d, the situation will be even worse because the effect of the above mentioned evanescent waves becomes stronger.

Moreover, the accuracy of the proposed model is verified for different incident angles. The reflected power in the previous example is once again plotted versus the incident angle at the normalized frequency $d/\lambda = 0.39$. The results are shown in figure 3. Evidently, the proposed model agrees well with the other two methods even for large values of θ.

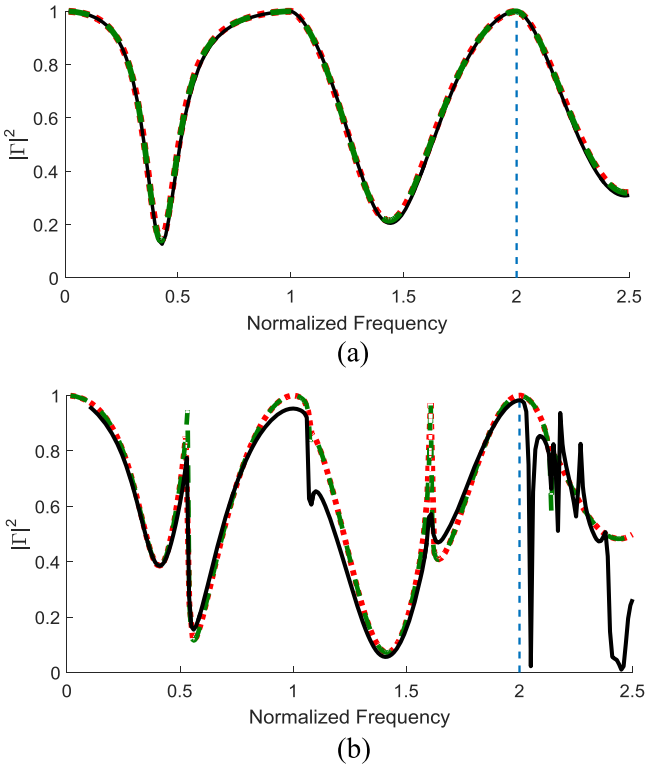

Figure 2. Reflected power from the graphene-covered metallic grating illuminated by an incident TM polarized wave versus the normalized frequency calculated by the full-wave simulations (solid), the TEM single mode approximation (dotted) and the proposed effective medium model (dashed). The incident angle is (a) $\theta = 0^\circ$ and (b) $\theta = 60^\circ$. The straight dashed line represents the maximum frequency limit obtained by the single mode approximation condition.

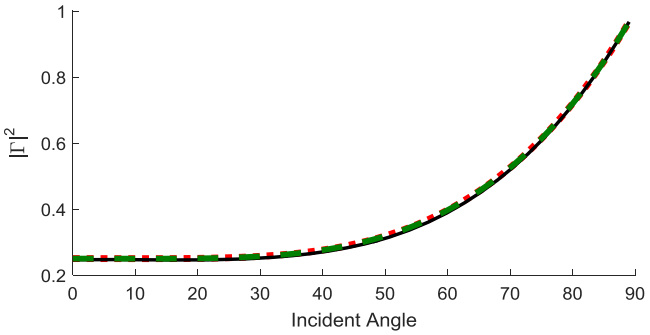

Figure 3. Reflected power from the graphene-covered metallic grating versus the incident angle calculated by the full-wave simulations (solid), the TEM single mode approximation (dotted) and the proposed effective medium model (dashed). The normalized frequency is $d/\lambda = 0.39$. The structure is illuminated by a TM polarized wave.

The accuracy of the proposed model when illuminated by a TE polarized wave incident at $\theta = 0^\circ$ and $\theta = 60^\circ$ is also evaluated in figure 4. It shows the reflected power obtained by the rigorous full-wave analysis (solid line), the single mode

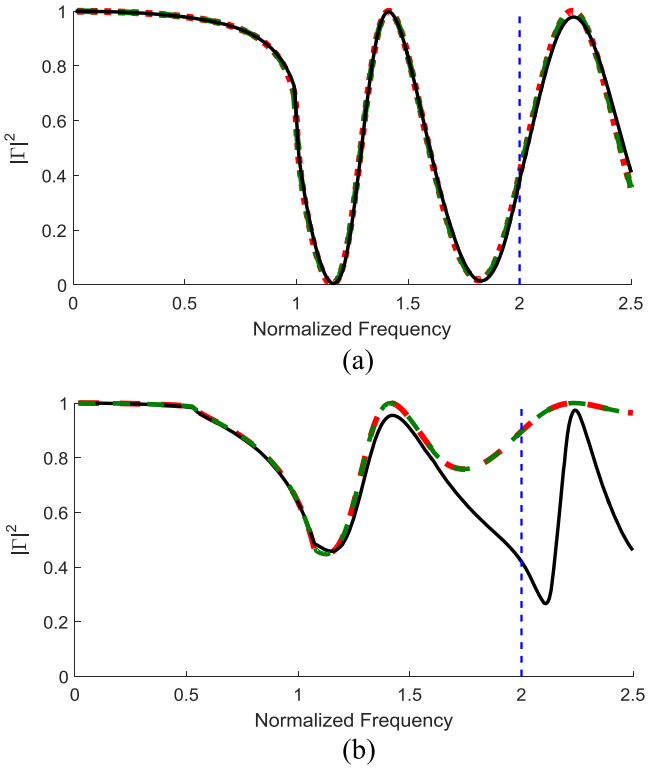

Figure 4. Reflected power from the graphene-covered metallic grating versus the normalized frequency calculated by the full-wave simulations (solid), the single mode approximation (dotted) and the proposed effective medium model (dashed). The structure is under illumination of a TE polarized wave. The incident angle is (a) $\theta = 0^\circ$ and (b) $\theta = 60^\circ$. The straight dashed line represents the maximum frequency limit obtained by the single mode approximation condition.

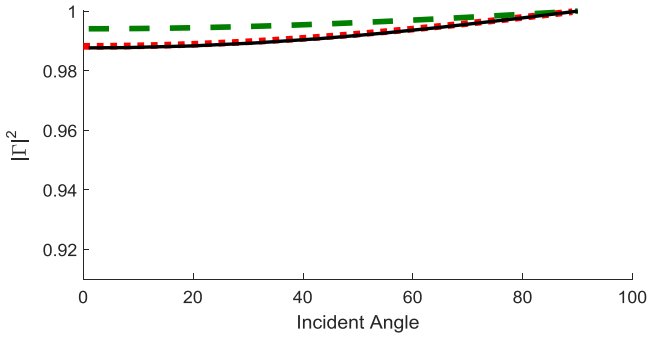

Figure 5. Reflected power from the graphene-covered metallic grating versus the incident angle calculated by the full-wave simulations (solid), the single mode approximation (dotted) and the proposed effective medium model (dashed). The normalized frequency is $d/\lambda = 0.4$. The structure is illuminated by a TE polarized wave.

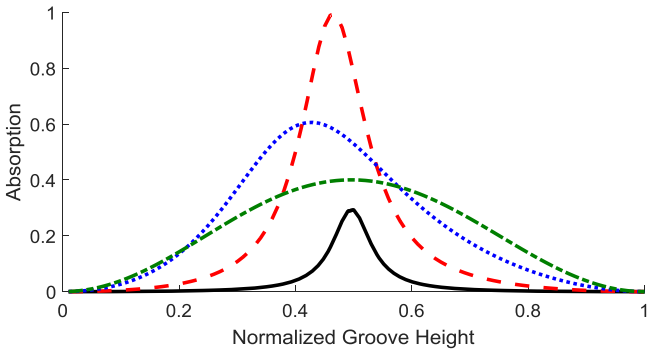

Figure 6. Absorption of the graphene-covered metallic grating calculated by the effective medium model versus the normalized groove height h/d and for different groove widths $a/d = 0.01$ (solid), $a/d = 0.1$ (dashed), $a/d = 0.5$ (dotted) and $a/d = 0.9$ (dashed-dotted). The normalized frequency is $d/\lambda = 0.5$ ($f = 0.75$ THz). The structure is illuminated by a normally incident TM polarized wave.

approximation inside the grooves, i.e. (24), (dotted line) and the proposed effective medium model (dashed line) versus the normalized frequency for the structure with parameters $n_1 = 1$, $n_2 = 1$, $d = 200$ μm, $h = 100$ μm and $a = 100$ μm. We marked the maximum frequency limit in which the proposed model remains valid based on the single model condition within each groove, i.e. $\lambda > an_2$, by a straight dashed line. The proposed model is in excellent agreement with the other two methods for the normalized frequencies lying within this limit.

Similar to the TM case, the validity of the proposed model is investigated for different incident angles. The reflected power in the previous example is once again plotted versus the incident angle at the normalized frequency $d/\lambda = 0.4$. The results are shown in figure 5.

Let us use this model to discuss the characteristics of an absorber which can effectively trap light in the THz frequency range. At first, the effects of geometrical parameters on the absorption are discussed. In figure 6, absorption which is calculated from one minus the reflected power is plotted versus the normalized groove height h/d for different values of groove width a in the structure with parameters $n_1 = 1$, $n_2 = 1$, $d = 200$ μm. Due to the weak coupling between the metallic grating and the graphene plasmons, absorption drastically decreases for very short and long groove widths. On the other hand, the resonance frequency of the structure is approximately constant for different groove widths. When the Fabry–Perot condition $\beta \times h = m\pi$ is satisfied, zero absorption is obtained in the structure. In contrast, by setting $\beta \times h = (m + 1/2)\pi$ and for a given factor a/d, we can maximize the absorption as the incident and the reflected waves interfere constructively at the openings of the grooves. It should be noted that β is the propagation constant of the TEM mode inside the grooves and m is an integer. Interestingly, a perfect absorption can be obtained for the TM polarization by tuning E_F and τ in (1).

To further discuss the enhanced absorption of graphene, another example is studied. Figure 7 depicts the absorption for normally incident TM waves both in the graphene-covered metallic grating (dashed-dotted line) and in the plain grating (dotted line) obtained by the effective medium model. The parameters of the structure are as follows: $n_1 = 1$, $n_2 = 1$, $d = 200$ μm, $h = 90$ μm and $a = 50$ μm and $E_F = 0.2$ eV. Evidently, for the normalized frequencies lying below unity, the presence of the graphene sheet invokes a near total absorption in the metallic grating while otherwise no

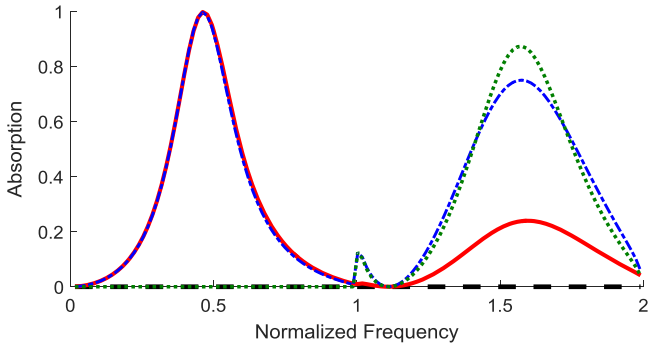

Figure 7. Absorption in the graphene-covered metallic grating (dashed-dotted) and the plain grating (dotted) obtained by the effective medium model versus the normalized frequency. Parameter α in the graphene-covered metallic grating (solid) and the plain grating (dashed) obtained by the full-wave simulations versus the normalized frequency. The dashed line is merged to the bottom x-axis due to zero absorption. The structure is illuminated by a normally incident TM wave.

absorption is seen in the plain grating. By further increasing the normalized frequency beyond unity, it can be observed that both structures can absorb a portion of the incident power. For $d/\lambda \geqslant 1$ in which, ± 1 st-order diffracted waves become propagating, some of the incident power is transmitted to the ± 1 st-reflected orders. In our model, which is characterized with homogenous media, the higher diffracted orders cannot exist. Therefore, the power carried by the higher order modes appears as a virtual absorption in the specular direction even in the plain grating. One can better understand this mechanism by plotting α defined as $\alpha = 1 - (DE_{r0}^{\mathrm{TM}} + DE_{r1}^{\mathrm{TM}} + DE_{r(-1)}^{\mathrm{TM}})$ versus the normalized frequency DE_{rn}^{TM} is the diffraction efficiency of nth order [31]. By using the full-wave simulations, α is plotted for the graphene-covered metallic grating (solid line) and the plain grating (dashed). In the former case, some of the incident power is absorbed by graphene (solid line). However, in the latter case, the absorption is zero and hence the dashed line is merged to the bottom x-axis. This is due to the fact that all of the incident power is reflected back to the free space in the specular (DE_{r0}^{TM}) and non-specular ($DE_{r(-1)}^{\mathrm{TM}}$ and DE_{r1}^{TM}) directions. Consequently, absorption is solely indebted to the plasmonic properties of graphene as long as the non-specular diffraction orders are evanescent. Higher diffraction orders also contribute to the absorption once they become propagating.

4. Conclusion

In this work, we proposed an effective medium model for the analysis of one-dimensional graphene-covered metallic gratings. This model consists of a dielectric slab that is covered by an effective surface conductivity. This surface conductivity incorporates the effects of the graphene sheet and those of the non-specular diffracted orders. Conductance of the above-mentioned surface conductivity and the effective relative permittivity of the slab have been given by explicit analytical expressions for both polarizations TM and TE, and for all incident angles. This model has been derived by assuming that only one mode is propagating inside the grooves. The accuracy of the proposed model has been demonstrated through several numerical examples and its limitations have also been clarified.

Using this model, it has been shown that the absorption of the graphene-covered metallic gratings substantially increases in comparison with that of the plain grating (for TM polarization). This is due to the strong coupling between the graphene plasmons and the evanescent waves diffracted by the metallic grating. These effects are summarized in the expression given for the effective surface conductivity. The absorption versus different parameters such as groove height and normalized frequency was also investigated.

This work provides a powerful tool for designing efficient absorbers or other novel devices based on the graphene-covered metallic gratings.

References

[1] Wang F, Zhang Y, Tian C, Girit C, Zettl A, Crommie M and Shen Y R 2008 Gate-variable optical transitions in graphene *Science* **2008** 206–9
[2] Novoselov K S, Fal V I, Colombo L, Gellert P R, Schwab M G and Kim K 2012 A roadmap for graphene *Nature* **490** 192–200
[3] Koppens F H, Chang D E and Garcia de Abajo F J 2011 Graphene plasmonics: a platform for strong light–matter interactions *Nano Lett.* **11** 3370–7
[4] Vakil A and Engheta N 2011 Transformation optics using graphene *Science* **332** 1291–4
[5] Bae S *et al* 2010 Roll-to-roll production of 30-inch graphene films for transparent electrodes *Nat. Nanotechnol.* **5** 574–8
[6] Xia F, Mueller T, Lin Y M, Valdes-Garcia A and Avouris P 2009 Ultrafast graphene photodetector *Nat. Nanotechnol.* **4** 839–43
[7] Bao Q and Loh K P 2012 Graphene photonics, plasmonics, and broadband optoelectronic devices *ACS Nano* **6** 3677–94
[8] Piper J R and Fan S 2014 Total absorption in a graphene monolayer in the optical regime by critical coupling with a photonic crystal guided resonance *ACS Photonics* **1** 347–53
[9] Zhao B, Zhao J M and Zhang Z M 2015 Resonance enhanced absorption in a graphene monolayer using deep metal gratings *J. Opt. Soc. Am.* B **32** 1176–85
[10] Liu X L, Zhao B and Zhang Z M 2015 Blocking-assisted infrared transmission of subwavelength metallic gratings by graphene *J. Opt.* **17** 035004
[11] Zhao B and Zhang Z M 2015 Strong plasmonic coupling between graphene ribbon array and metal gratings *ACS Photonics* **2** 1611–8
[12] Zhao B, Zhao J M and Zhang Z M 2014 Enhancement of near-infrared absorption in graphene with metal gratings *Appl. Phys. Lett.* **105** 031905
[13] Amin M, Farhat M and Bağcı H 2013 An ultra-broadband multilayered graphene absorber *Opt. Express* **21** 29938–48
[14] Andryieuski A and Lavrinenko A V 2013 Graphene metamaterials based tunable terahertz absorber: effective surface conductivity approach *Opt. Express* **21** 9144–55
[15] Jang M S, Brar V W, Sherrott M C, Lopez J J, Kim L, Kim S, Choi M and Atwater H A 2014 Tunable large resonant absorption in a midinfrared graphene Salisbury screen *Phys. Rev.* B **90** 165409
[16] Nikitin A Y, Guinea F, Garcia-Vidal F J and Martin-Moreno L 2012 Surface plasmon enhanced absorption and suppressed

transmission in periodic arrays of graphene ribbons *Phys. Rev.* B **85** 081405
[17] Xu B Z, Gu C Q, Li Z and Niu Z Y 2013 A novel structure for tunable terahertz absorber based on graphene *Opt. Express* **21** 23803–11
[18] Alaee R, Farhat M, Rockstuhl C and Lederer F 2012 A perfect absorber made of a graphene micro-ribbon metamaterial *Opt. Express* **27** 28017–24
[19] Christensen J, Manjavacas A, Thongrattanasiri S, Koppens F H and García de Abajo F J 2011 Graphene plasmon waveguiding and hybridization in individual and paired nanoribbons *ACS Nano* **6** 431–40
[20] Khavasi A and Rejaei B 2014 Analytical modeling of graphene ribbons as optical circuit elements *IEEE J. Quantum Electron.* **50** 397–403
[21] Khavasi A 2015 Design of ultra-broadband graphene absorber using circuit theory *J. Opt. Soc. Am.* B **32** 1941–6
[22] Thongrattanasiri S, Koppens F H and de Abajo F J 2012 Complete optical absorption in periodically patterned graphene *Phys. Rev. Lett.* **108** 047401
[23] Fallahi A and Perruisseau-Carrier J 2012 Design of tunable biperiodic graphene metasurfaces *Phys. Rev.* B **86** 195408
[24] Ebbesen T W, Lezec H J, Ghaemi H F, Thio T and Wolff P A 1998 Extraordinary optical transmission through sub-wavelength hole arrays *Nature* **391** 667–9
[25] Yee K S 1966 Numerical solution of initial boundary value problems involving Maxwell's equations in isotropic media *IEEE Trans. Antennas Propag.* **14** 302–7
[26] Edalatipour M, Khavasi A, Rezaei M and Mehrany K 2012 Creation of artificial surface conductivity on metallic metamaterials *J. Lightwave Technol.* **30** 1789–94
[27] Yarmoghaddam E, Shirmanesh G K, Khavasi A and Mehrany K 2014 Circuit model for periodic array of slits with multiple propagating diffracted orders *IEEE Trans. Antennas Propagation* **62** 4041–8
[28] Yang R, Rodríguez-Berral R, Medina F and Hao Y 2011 Analytical model for the transmission of electromagnetic waves through arrays of slits in perfect conductors and lossy metal screens *J. Appl. Phys.* **109** 103107
[29] Rodríguez-Berral R, Mesa F and Medina F 2010 Circuit model for a periodic array of slits sandwiched between two dielectric slabs *Appl. Phys. Lett.* **96** 161104
[30] Khavasi A and Mehrany K 2011 Circuit model for lamellar metallic gratings in the sub-wavelength regime *IEEE J. Quantum Electron.* **47** 1330–5
[31] Moharam M G, Gaylord T K, Grann E B and Pommet D A 1995 Formulation for stable and efficient implementation of the rigorous coupled-wave analysis of binary gratings *J. Opt. Soc. Am.* A **12** 1068–76